Progress In Electromagnetics Research M, Vol. 118, 137–149, 2023

Simultaneous Detection of CO_2 and N_2O Based on Quartz-Enhanced Photothermal Spectroscopy by Using NIR and MIR Lasers

Fangmei Li[1, 2], Tie Zhang[1, 2], Gaoxuan Wang[1, 3], and Sailing He[1, 2, 3, *]

Abstract—Quartz-enhanced photothermal spectroscopy (QEPTS) technique is suitable for simultaneous measurement of multi-gas in near-infrared (NIR) and mid-infrared (MIR) bands with advantages of wide spectral response and high sensitivity. Here, we report a multi-gas sensing system based on QEPTS using NIR and MIR Lasers. A quartz tuning fork (QTF) with a resonant frequency f_0 of 32.742 kHz was employed as a photothermal detector. A continuous wave distributed feedback (CW-DFB) fiber-coupled diode laser with a center wavelength of 1.58 µm and an interband cascade laser (ICL) with a center wavelength of 4.47 µm were used as the light sources to simultaneously irradiate on different surfaces of QTF for scanning the absorption lines of carbon dioxide (CO_2) and nitrous oxide (N_2O). A multi-pass cell with an effective optical path of 40 m and a 40 cm absorption cell were selected for the measurements of CO_2 and NO_2, respectively. The developed sensor was validated by the detection of mixtures containing 3000 ppm CO_2 and 20 ppm N_2O. The relationships between the second harmonic (2f) amplitude of the QEPTS signal and the CO_2 and N_2O concentrations were investigated. Allan deviation analysis showed that this sensor had excellent stability and high sensitivity with a minimum detection limit (MDL) of 2.729 ppm for CO_2 in an integration time of 195 s and 0.038 ppb for N_2O in an integration time of 90 s, respectively.

1. INTRODUCTION

Climate change can accelerate glaciers melting, rising sea levels, droughts and floods, etc. [1–6], which generates adverse effects on environment quality and socioeconomic development. Carbon dioxide (CO_2) is responsible for 55–60% of current anthropogenic radiative forcing on warming impact, and the warming potential of nitrous oxide (N_2O) is 298 times that of CO_2 [7]. The Intergovernmental Panel on Climate Change (IPCC) reports that human activities, such as agricultural production, industrial production, and domestic waste treatment activities [8, 9], are the main reasons for increasing the concentration of atmospheric greenhouse gases. In addition, the detection of CO_2 concentration exhaled from the human body can be used for cardiopulmonary functional assessment in the medical field [10, 11]. Therefore, the development of CO_2 and N_2O sensors with high sensitivity is of great significance for global warming and medical diagnosis.

Gas sensors are generally classified as non-optical sensor and optical sensor. Non-optical sensor such as electrochemical and semiconductor sensors is based on chemical processes and electrical properties to detect gases with an advantage of low-cost [12, 13]. Optical sensor is mainly based on light-matter interaction including absorption, scattering, and extinction [14, 15], and is widely used in numerous fields of biomedical analyses [16, 17], environmental monitoring [18, 19], and combustion diagnosis [20–22] with advantages of fast response, high sensitivity and selectivity, real-time detection, etc. [23–26].

Received 8 July 2023, Accepted 9 August 2023, Scheduled 28 August 2023

* Corresponding author: Sailing He (sailing@zju.edu.cn).

[1] Centre for Optical and Electromagnetic Research, National Engineering Research Center for OpticalInstruments, Zhejiang Provincial Key Laboratory for Sensing Technologies, College of Optical Science and Engineering, Zhejiang University, Hangzhou 310058, China. [2] Research Institute of Zhejiang University-Taizhou, China. [3] Ningbo Research Institute, Zhejiang University, Ningbo 315100, China.

Several optical absorption spectroscopy techniques have been developed, such as tunable diode laser absorption spectroscopy (TDLAS) and photoacoustic spectroscopy (PAS) [27–29]. Each technique has its own limitations for multi-gas detection. Photoacoustic spectroscopy is recognized as one of the most promising absorption spectroscopy methods. Traditional PAS method is based on cylindrical resonator, but the low resonance frequency and low quality factor (< 100) of cylindrical resonator cause poor signal-to-noise ratio (SNR) for the sensor system [27].

Quartz-enhanced photoacoustic spectroscopy (QEPAS), with a high quality factor of $\sim 100,000$, provides an effective improvement of the PA sensor performance compared to the traditional PAS [30]. QEPAS uses a quartz tuning fork (QTF) as an acoustic wave detector. The sound wave generated by the target gas after absorbing photonic energy causes vibration of QTF, which results in the variation of piezoelectric charge due to the piezoelectric effect of QTF [31]. However, as a contact detection method, QEPAS [32] requires the QTF to be placed in the target gas environment, which deteriorates the performance of the resonance characteristic and quality factor of the QTF due to the corrosive gases in some specific applications, such as corrosive gases measurement and combustion diagnosis [33].

Unlike QEPAS, quartz-enhanced photothermal spectroscopy (QEPTS) is a non-contact measurement method, which uses the QTF as a photothermal detector. The modulated photonic radiation is absorbed by the QTF to generate thermal wave. The thermoelastic expansion converts the thermal energy to deformation, which causes mechanical motion of QTF. Owing to the piezoelectric effect of the QTF, the mechanical motion produces a piezoelectric charge on the surface of QTF, which is eventually converted into an electrical signal containing information about the gas concentration. When the modulation frequency of the absorbed photonic radiation is consistent with the resonant frequency of QTF, the mechanical motion of the QTF reaches the maximum value with a high piezoelectric signal [31]. As the QTF can be placed after the absorbed light by the target gas in QEPTS, so it is advantageous for combustion diagnosis and the detection of corrosive gases such as H_2S [34] and HCl [35], compared with QEPAS. Furthermore, the detection performance of QEPTS can be improved by increasing the effective optical path.

Many methods have been proposed for improving the performance of QEPTS. He et al. [36] successfully improved the performance of the QEPTS by placing the QTF in a low-pressure environment and using a multi-pass cell (MPC) with an effective optical path of 10 m, and a normalized noise equivalent absorption coefficient (NNEA) of $7.4 \times 10^{-10}\,\mathrm{cm^{-1}\cdot W\cdot Hz^{-1/2}}$ was obtained. In 2020, Ma et al. [37] reported a multi-quartz-enhanced photothermal spectroscopy (M-QEPTS) using two QTFs as the photothermal detectors, and an enhancement of 1.51 times was achieved compared to the traditional single QTF sensing system. A long-path QEPTS gas sensor using a Q-switched fiber laser and a circulator was proposed by Zhang et al. in 2020 [20]. A minimum detection limit (MDL) of 6.1 ppb with a integration time of 48 s was obtained for acetylene (C_2H_2) detection [38]. Zhou et al. [39] greatly enhanced the light absorption efficiency by plating a thin film on the surface of QTF, and the MDL reached 0.88 ppm for methane (CH_4) detection. A trace gas detection technique of quartz-enhanced photoacoustic-photothermal spectroscopy (QEPA-PTS), which combined the advantages of QEPAS and QEPTS by using two QTFs, was demonstrated by Hu et al. [40]. In 2022, a custom low-frequency QTF was adopted to achieve a longer energy accumulation time, and ~ 2 times signal amplitude enhancement was achieved compared to the standard 32 kHz QTF [35].

In this paper, a CO_2 and N_2O sensor based on QEPTS using NIR and MIR lasers is proposed. This paper firstly focuses on simultaneously exploiting the front and back surfaces of the QTF for simultaneous measurement of multiple gases in NIR and MIR bands. A QTF with a resonant frequency f_0 of 32 kHz was used as a photothermal detector, which had an excitation source on each side. On one surface of the QTF, a distributed feedback (DFB) laser with a center wavelength of 1.58 μm was used as an excitation source after passing an MPC with an effective optical path of 40 m. On another surface, an interband cascade laser (ICL) with a center wavelength of 4.47 μm was used as an MIR excitation source, and a 40 cm gas cell was adopted for measuring N_2O. The response of the QTF sensor was investigated when two excitation sources were simultaneously irradiated on the different surfaces of QTF. CO_2 and N_2O were simultaneously measured to validate the detection performance of the sensing system. Wavelength modulation spectroscopy with second-harmonic detection (WMS-2f) was used to improve the detection sensitivity, and the current modulation amplitude was optimized.

2. EXPERIMENTAL SETUP

2.1. Absorption Lines Selection

The sensitivity of an optical gas sensor based on the absorption spectroscopy highly depends on the chosen absorption line of the target gas analyte. The spectral absorption interference from other atmospheric composition will reduce the measurement accuracy. Figure 1(a) shows the simulated absorption cross-section of CO_2 and N_2O from 1000 to 6000 cm^{-1}, according to the HITRAN database [41]. N_2O has strong absorption in the MIR region, and the absorption peak intensity can reach 10^{-18} cm^2/molecule at 2238.36 cm^{-1}, which is selected for measuring N_2O using a 2237 cm^{-1} interband cascade laser. Although CO_2 has the strongest absorption in the MIR region around 2364 cm^{-1}, a long-path cell can be used to achieve a high sensitivity for a spectroscopic sensor using the WMS-2f technique near 6250 cm^{-1}, and an absorption line of 10^{-18} cm^2/molecule at 6330.82 cm^{-1} is chosen finally in the present paper. Considering the cost and sensitivity, a 6329 cm^{-1} DFB laser is selected for CO_2 measurement, and a 40 m multi-pass cell is adopted to achieve high sensitivity detection. The absorbance spectra of CO_2, N_2O, and H_2O simulated in selected wavenumber range are shown in Figures 1(b), (c), where one can see that there is no interference between the selected gas analytes.

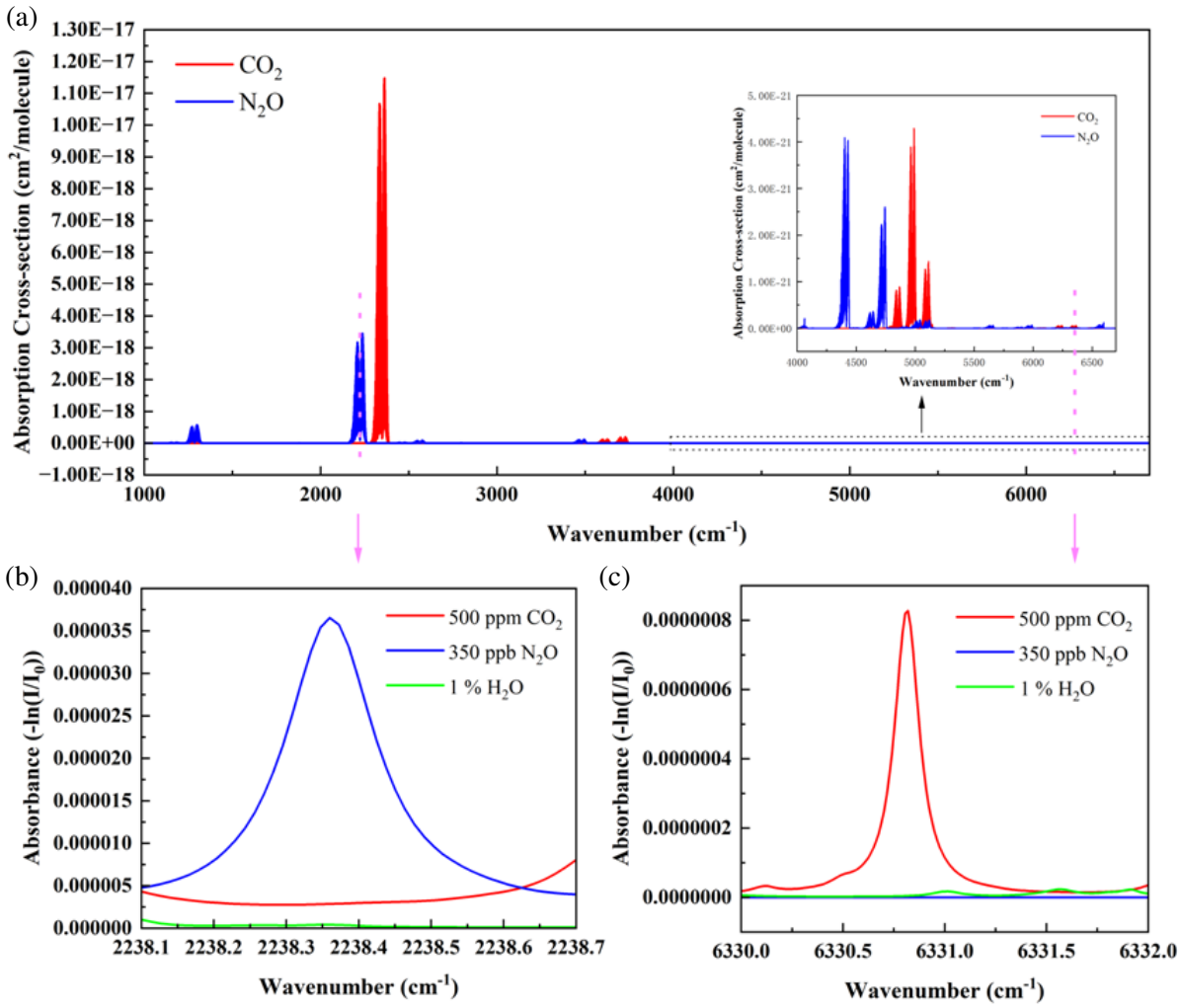

Figure 1. (a) The simulated absorption cross-section of CO_2 and N_2O from 1000 to 6000 cm^{-1} based on HITRAN database [41]. The absorbance spectra of 500 ppm CO_2, 350 ppb N_2O and 1% H_2O at 296 K temperature, 1 atm pressure and 1 cm absorption path length in the selected wavenumber range of (b) 2238.1 cm^{-1} ~ 2238.7 cm^{-1} and (c) 6330 cm^{-1} ~ 6332 cm^{-1}.

2.2. Sensor Configuration

The experimental setup for the reported multi-gas CO_2/N_2O sensor based on QEPTS is shown in Figure 2. Two excitation sources and two gas cells were adopted. A near-infrared continuous wave distributed feedback (CW-DFB) fiber-coupled diode laser with a center wavelength of 1.58 µm and optical power of 20 mW was selected as one of the excitation sources. An optical fiber connector was used to send laser beam 1 (emitted from the DFB laser) to a fiber-coupled MPC with an effective optical path of 40 m. A mid-infrared interband cascade laser (Nanosystems and Technologies GmbH, GRE) with a center wavelength of 4.47 µm and optical power of 5 mW was selected as another excitation source. A collimator (C028TME-E, Thorlabs, Newton, USA) was used to collimate the laser beam 2 which was sent into a 40 cm absorption cell. The current and temperature of the two lasers were controlled by two laser drivers (LDC 205C and TED200C, Thorlabs, Newton, USA), for covering the selected absorption lines of CO_2 and N_2O. After the mass flow controller (MPC), a collimator (F280APC-1550, Thorlabs, Newton, USA) and a lens with a focal length of 75 mm were used to focus laser beam 1 on the root of one surface of the QTF. The laser beam 2 was focused on the root of another surface of the QTF by a lens with 25 mm focal length, after passing through the absorption cell. A QTF with a resonant frequency f_0 of $\sim$ 32 kHz was employed, and a XYZ translator was used to adjust the laser irradiation position. CO_2, N_2O, and pure nitrogen (N_2) were used to produce gas mixtures of different proportions by three MFCs.

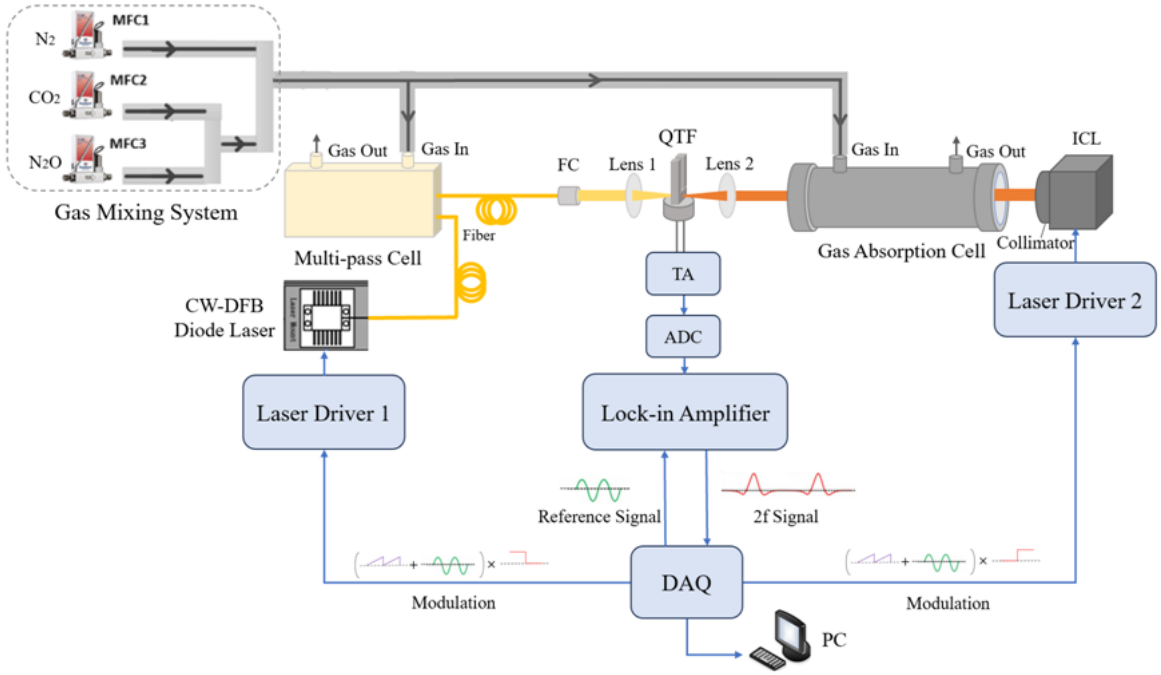

Figure 2. Schematic diagram of the experimental setup. QTF, quartz tuning fork; ICL, interband cascade laser; FC, fiber collimator; TA, trans-impedance amplifier; ADC, analog-to-digital converter; DAQ, data acquisition card; MFC, mass flow controller; PC, personal computer.

Accurate detection was realized through wavelength modulation spectroscopy with second-harmonic detection (WMS-2f). A DAQ card (USB-6229, National instrument, Austin, TX, USA) was used to generate two analog signals and modulate the wavelength of two lasers through laser drivers, respectively. As shown in Figure 3, the modulation signals were based on a high-frequency sine wave ($f = f_0/2$) and a low-frequency sawtooth wave, and then combined with a square wave. In a scan period of 5 s, the near-infrared and mid-infrared lasers were each scanned for 2.5 s to achieve the simultaneous measurement of CO_2 and N_2O in the same period. Moreover, a reference signal was also generated by the DAQ to demodulate the detection signal using a lock-in amplifier. The integration time of the lock-in amplifier was set to 200 ms. The demodulated result was displayed by a LABVIEW program.

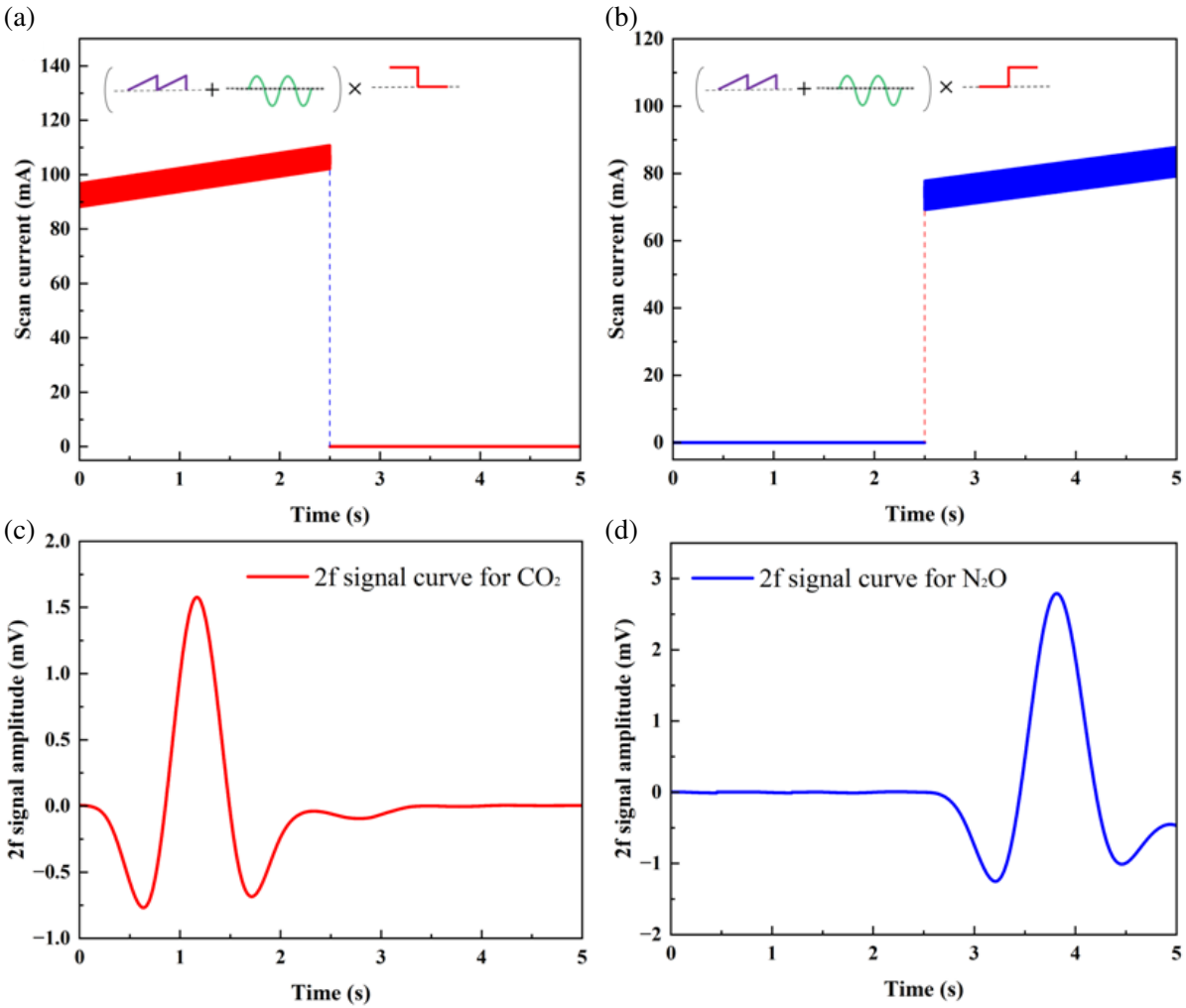

Figure 3. Schematic diagram of the scanning currents of the (a) near-infrared and (b) mid-infrared lasers. 2f signal measured by the (c) near infrared and (d) mid-infrared lasers, corresponding to the target absorption lines of CO_2 and N_2O, respectively.

3. EXPERIMENTAL RESULTS AND DISCUSSIONS

3.1. QTF Characteristic Research

An optical excitation method using periodic electromagnetic wave to illuminate one surface of the QTF was adopted to test the used QTF under atmospheric pressure. Figure 4 shows the standardized frequency response curve of QTF, and the resonance frequency f_0 is 32742 Hz. Due to the interference of the experimental environment, the resonance profile seemed asymmetric. But this had no effect on the overall experiment, and only the peak value was noteworthy.

The frequencies of Laser 1 and Laser 2 were both set to 16371 Hz, half of the resonant frequency of the QTF, to obtain the signals generated by the QTF. Two infrared sensing cards with different coverage bands were used to roughly focus the two lasers near the QTF, and then an XYZ translator was used to adjust the position of the QTF precisely. The light spots of the two laser sources were focused on the roots of different surfaces of QTF, the optimum irradiation point [36] by observing the signal of the lock-in amplifier, and the vibration directions of QTF caused by the two laser sources were always consistent. The piezoelectric signals generated by QTF would weaken each other when the vibration directions were different; only when the vibration directions were consistent, the piezoelectric

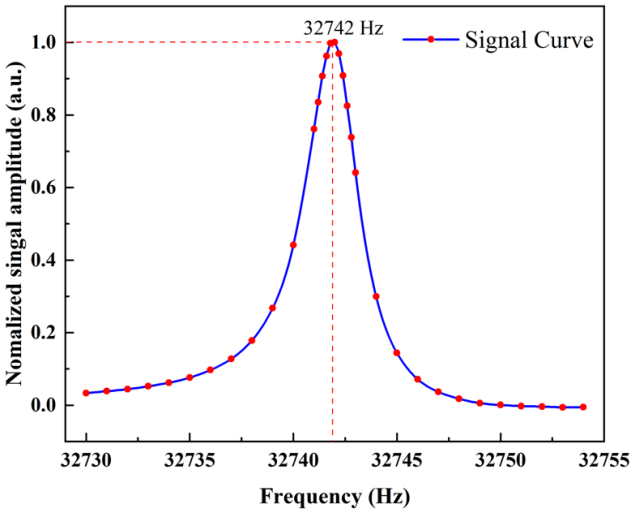

Figure 4. Peak-normalized data of the frequency response for the selected QTF.

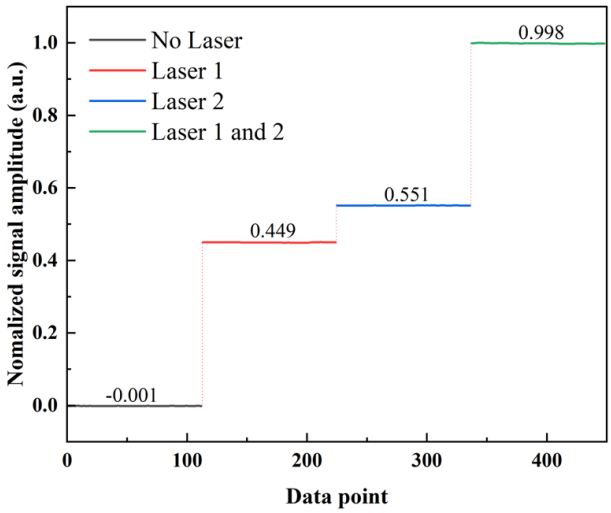

Figure 5. The piezoelectric signals generated by QTF with no laser irradiation, two laser beams separately and simultaneously irradiating on the different surfaces of QTF.

signals could be superimposed. As shown in Figure 5, the piezoelectric signals generated by QTF were recorded with no laser irradiation, with two laser beams separately and simultaneously irradiating on the different surfaces of QTF. The results showed that the piezoelectric signal of QTF simultaneously irradiated by two lasers was the sum of the piezoelectric signal separately irradiated by two lasers, which proved that it is feasible to measure multi-gas utilizing different surfaces of QTF in this paper.

3.2. Modulation Amplitude Optimization

To scan the absorption line of CO_2 molecule, the initial current and temperature of the DFB laser were set to 92.5 mA and 28.6°C, respectively. The amplitude of the sawtooth wave and sine wave varied from 0 to 280 mV and −90 to 90 mV, respectively. The initial current and temperature of the ICL were set to

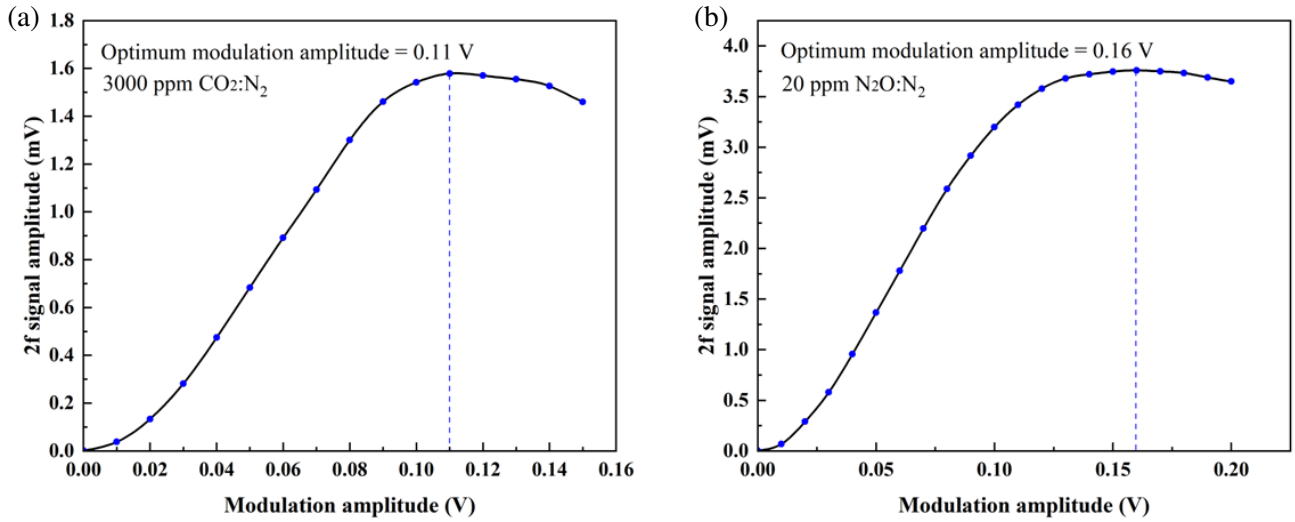

Figure 6. The QEPTS-2f signal amplitudes of (a) CO_2 and (b) N_2O as the modulation amplitude varies.

73.5 mA and 17.7°C, respectively. The amplitude of the sawtooth wave and sine wave were respectively varied from 0 to 200 mV and −90 to 90 mV to scan the absorption line of N_2O molecule. The modulation coefficient of laser drivers is 50 mA/V, which leads to the injected current of the DFB laser varied from 92.5 to 106.5 mA, and the injection current of ICL varied from 73.5 to 83.5 mA. The frequencies of the sawtooth waves were both set to 200 mHz resulting in a total scan period of 5 s. The frequencies of the sine signals were both set to 16371 Hz, which was half of the QTF resonance frequency. The two modulation signals were further superimposed with two square waves of opposite phases, respectively. In the 5 s scanning period, the DFB laser only scanned the first 2.5 s, and the ICL only scanned the last 2.5 s, as shown in Figure 3.

The modulation amplitude has great influence on the experimental results. The detection of 3000 ppm CO_2 and 20 ppm N_2O was carried out to obtain the optimal modulation amplitude of CO_2 and N_2O. Figure 6(a) plots the relationship between the QEPTS-2f signal amplitude and the current modulation amplitude of the 1.58 µm laser. Figure 6(b) plots the relationship between the QEPTS-2f signal amplitude and the current modulation amplitude of the 4.47 µm laser in a N_2O environment. With the increase of modulation amplitude, the QEPTS-2f signal amplitude firstly increased and then decreased. The QEPTS-2f signal amplitude of CO_2 and N_2O reached the maximum value with the

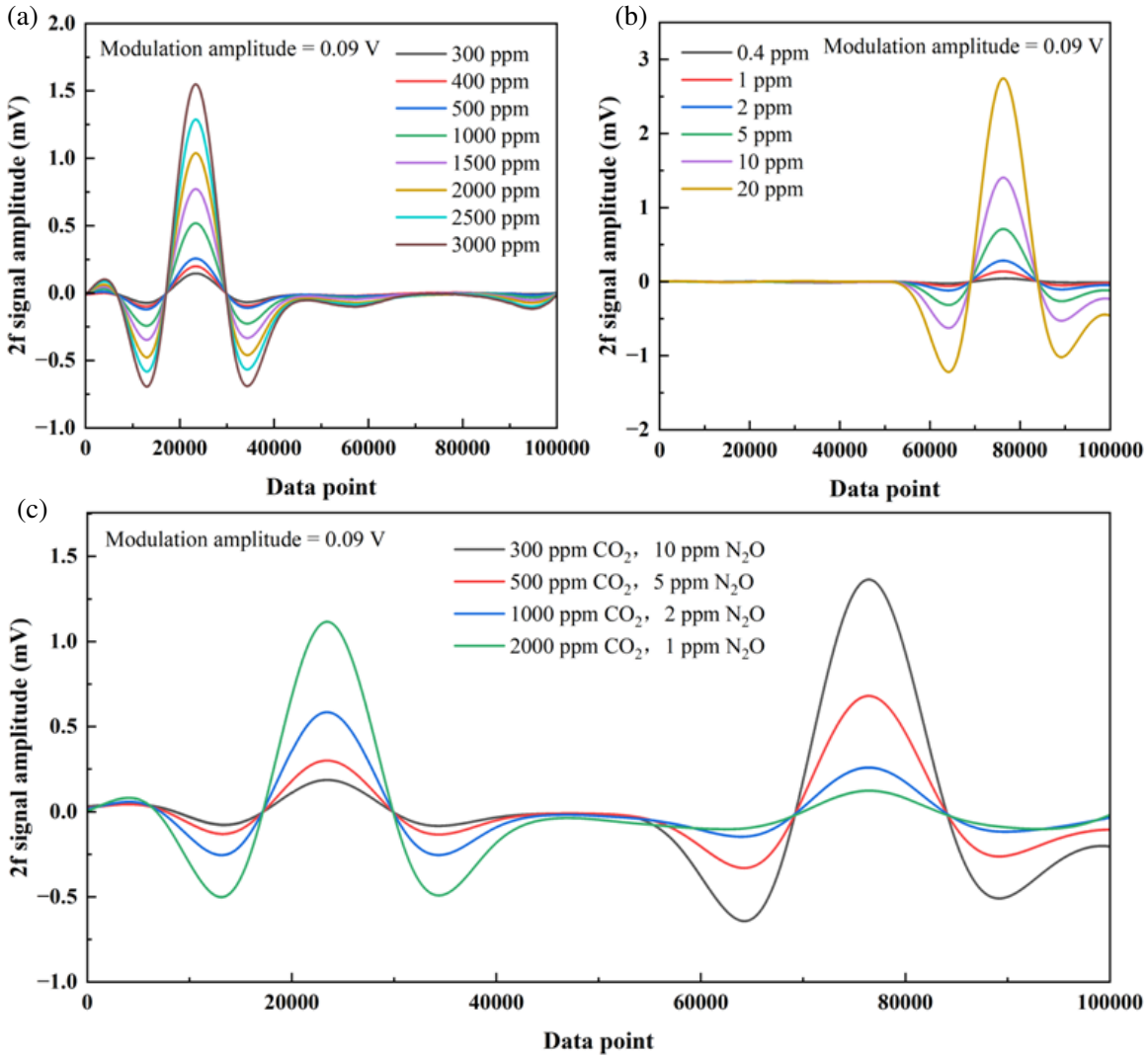

Figure 7. The QEPTS-2f signals measured when the gas cell was filled with (a) CO_2, (b) N_2O, and (c) a gaseous mixture of CO_2 and N_2O, with different concentrations.

modulation amplitude of 0.11 V and 0.16 V, respectively. However, the 2f signal was gradually widened with the increase of modulation amplitude, which is not conducive to the simultaneous display of CO_2-QEPTS 2f signal and N_2O-QEPTS 2f signal. The modulation amplitude of 90 mV was finally selected.

3.3. Linear Calibration

For the simultaneous measurement of CO_2 and N_2O, two mixed-gas cylinders of 3000 ppm CO_2 and 20 ppm N_2O were used. The two gas cells in the sensor system were always flushed with the same gaseous mixture. Figures 7(a) and (b) show the 2f signals with different CO_2 or N_2O concentrations. Figure 7(c) shows the 2f signals when the gas cells were filled with different concentrations of CO_2 and N_2O simultaneously. As the gas concentration increases, the 2f signal amplitudes also increase. The detected signals of CO_2 and N_2O do not affect each other.

The measurement interference of CO_2 and N_2O on each other was investigated as shown in Figure 8. Figure 8(a) shows the measured QEPTS-2f signals with the concentration of CO_2 varying from 300 to 2000 ppm and a constant N_2O concentration of 2 ppm. A linear fit of the peak values of CO_2 signal

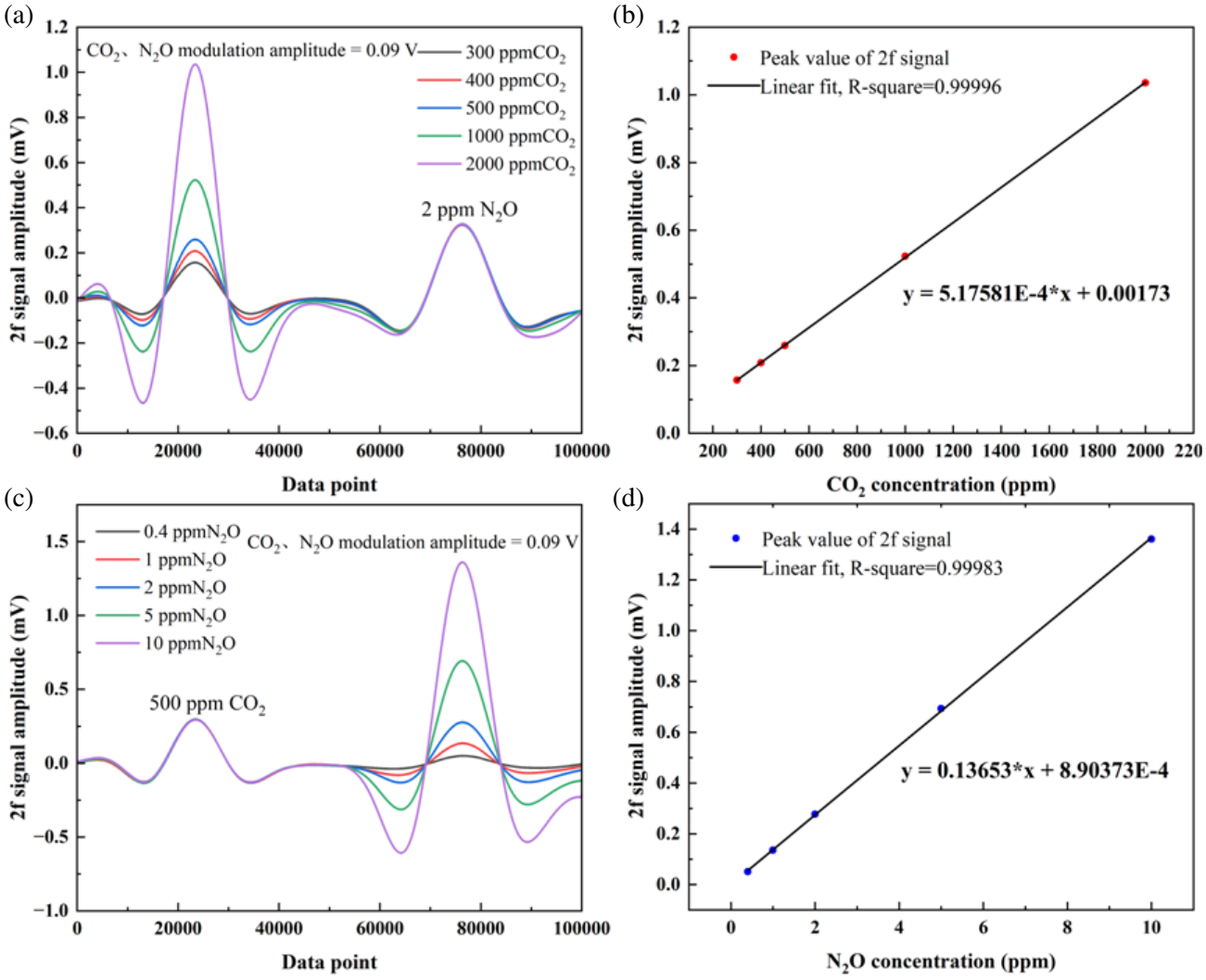

Figure 8. (a) QEPTS-2f signals at different CO_2 concentrations with a constant N_2O concentration of 2 ppm, and (b) the corresponding linear fitting. (c) QEPTS-2f signals at different N_2O concentrations with a constant CO_2 concentration of 500 ppm, and (d) the corresponding linear fitting.

on different CO_2 concentrations is plotted in Figure 8(b). Figure 8(c) shows the measured QEPTS-2f signals with the concentration of N_2O varying from 0.4 to 10 ppm and a constant CO_2 concentration of 500 ppm. A linear fit of the peak values of N_2O signal on different N_2O concentrations is plotted in Figure 8(d). The R-square is 0.99996 for CO_2 and 0.99983 for N_2O. These results show that the QEPTS sensor has an excellent linear response for the detection of CO_2 and N_2O.

Figure 9(a) shows the measurement results when the concentration of N_2O is constant, and the concentration of CO_2 varies from 2000 to 300 ppm. The blue line represents the retrieved N_2O concentrations using the linear regression equation, which were not affected by CO_2 concentrations. Figure 9(b) shows the measurement results when the concentration of CO_2 is constant, and the concentration of N_2O varies from 10 to 0.4 ppm, where the red line indicates that the measurement of CO_2 would not be affected by different N_2O concentrations. The error of the mass flow controllers may be the cause of the gap between the retrieved concentration and the actual concentration of CO_2 and N_2O.

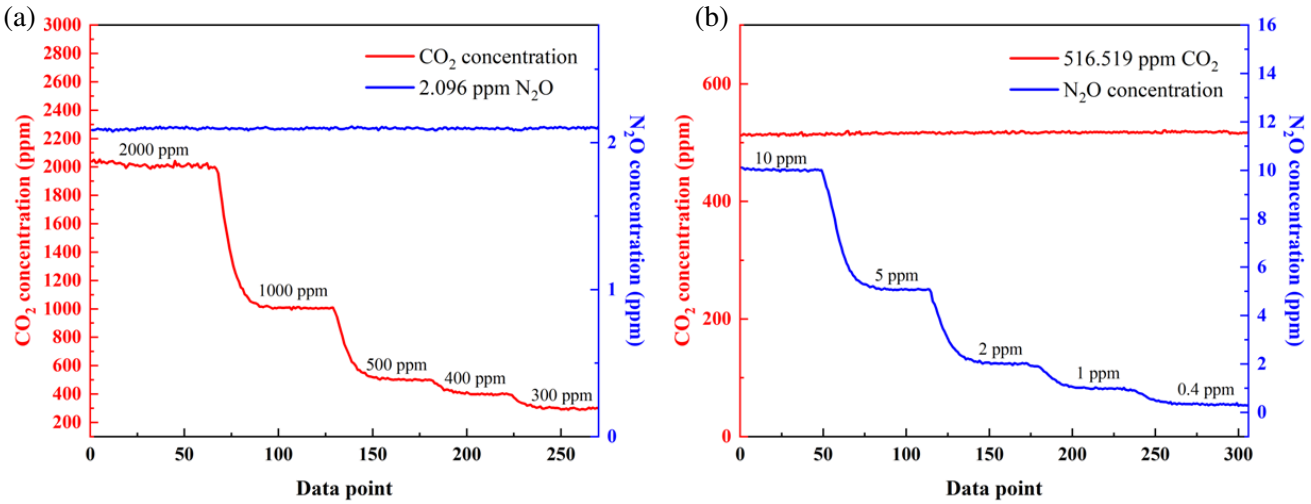

Figure 9. (a) Measurement results when the concentration of N_2O is constant and the concentration of CO_2 varies from 2000 to 300 ppm. (b) Measurement results when the concentration of CO_2 is constant and the concentration of N_2O varies from 10 to 0.4 ppm.

3.4. Allan Deviation Analysis

The stability of the system was evaluated by an Allan deviation analysis. The gas cells were always kept at a gas flow rate of 0.9 L/min. 1500 ppm CO_2 gas and 5 ppm N_2O gas were obtained to finish the experiment. As shown in Figures 10(a) and (b), under this condition, CO_2 and N_2O were continuously measured over 4000 s, and a data point for CO_2 and N_2O concentrations was respectively obtained every 5 s. The concentrations were from 1525 to 1554 ppm for CO_2 measurement, and the measurement error was $\pm 2.7\%$. The concentrations for N_2O measurement were from 5.35 to 5.47 ppm, and the measurement error was $\pm 8.7\%$. Figures 10(c) and (d) show that the detection sensitivities of CO_2 and N_2O were 43.329 ppm and 0.597 ppb, respectively, in 5 s averaging time. When the averaging time was 195 s, the sensitivity of CO_2 improved to 2.729 ppm, and when the averaging time was 90 s, the sensitivity of N_2O improved to 0.038 ppb. This means that the gas sensing system has a good stability.

3.5. Detection of Ambient CO_2 and N_2O

The practical application capability of the multi-gas sensing system was evaluated by detecting CO_2 and N_2O in the surrounding environment. The experiment was carried out indoors. As shown in Fig. 11, the measured QEPTS-2f signal peaks of CO_2 and N_2O were 0.25 mV and 0.046 mV, respectively, and the retrieved concentrations were 479.712 ppm for CO_2 and 331 ppb for N_2O using the linear regression

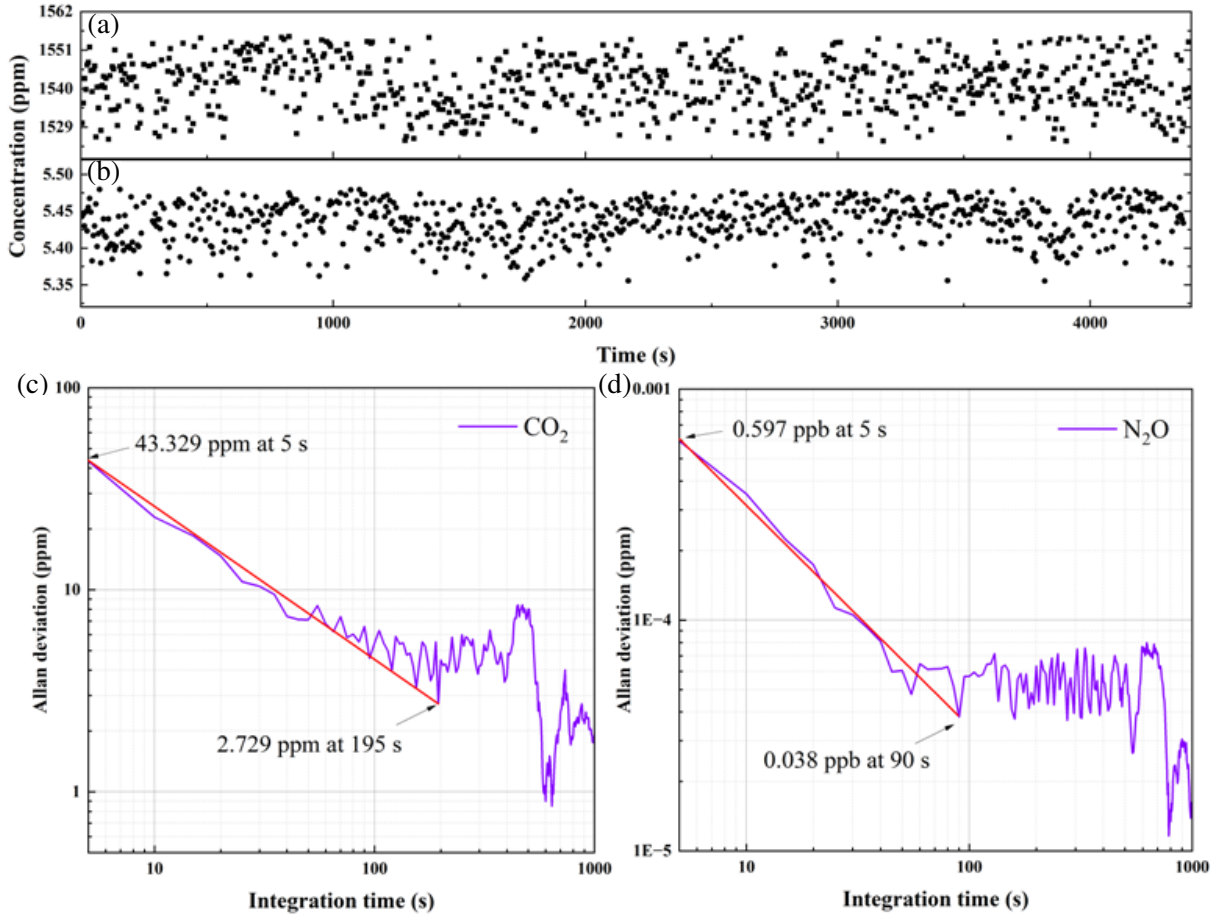

Figure 10. Measured (a) CO_2 concentrations of 1500 ppm and (b) N_2O concentrations of 5 ppm. Allan deviation plot as a function of the integration time for (c) CO_2 and (d) N_2O.

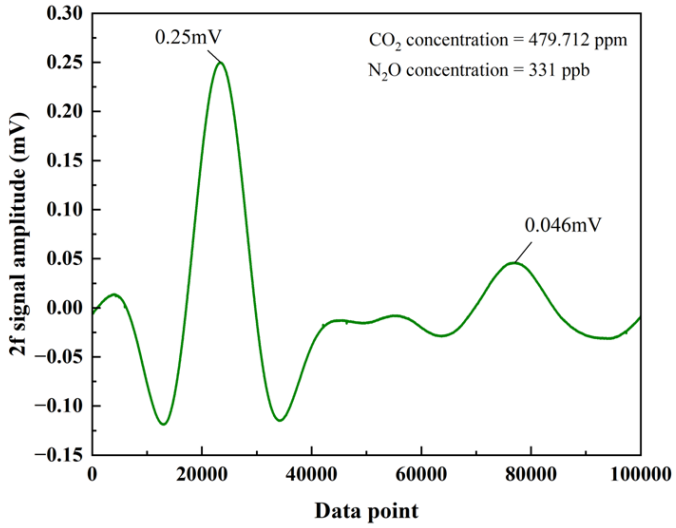

Figure 11. Measured QEPTS-2f spectral signal of CO_2 and N_2O in an indoor environment.

equation. Taking into account the human activities and the air circulation system in the laboratory, the measurement results are consistent with the concentration levels of CO_2 and N_2O in the atmosphere.

4. CONCLUSIONS

In this paper, we have achieved simultaneous detection of CO_2 and N_2O using a QEPTS-based multi-gas sensing system. A QTF with a resonant frequency f_0 of 32.742 kHz has been employed as a photothermal detector. A near-infrared CW-DFB fiber-coupled diode laser with a center wavelength of 1.58 µm and a mid-infrared ICL with a center wavelength of 4.47 µm, for covering the absorption lines of CO_2 and N_2O, have been adopted as the excitation sources to simultaneously irradiate on different surfaces of the QTF. We have shown that the piezoelectric signal of QTF simultaneously irradiated by two lasers was the sum of the piezoelectric signal separately irradiated by two lasers, which proved that it is feasible to measure multiple gases utilizing different surfaces of QTF. A multi-pass cell with an effective optical path of 40 m and a 40 cm absorption cell were selected as the gas cells. A mixture of 3000 ppm CO_2 and 20 ppm N_2O was adopted as the analyte. Wavelength modulation spectroscopy with second-harmonic detection (WMS-2f) was utilized to improve detection sensitivity for the target gas. The optimized current modulation amplitude was 90 mV. This QEPTS sensor had a good linear response with CO_2 and N_2O concentration, and the R-square value reached 0.99996 and 0.99983, respectively, which proved the reliability of the system. Allan deviation analysis showed that this sensor had excellent stability and high sensitivity. The detection limits of 43.329 ppm for CO_2 and 0.597 ppb for N_2O were achieved at an averaging time of 5 s. The detection sensitivity can be improved to 2.729 ppm for CO_2 and 0.038 ppb for N_2O at an optimal averaging time of 195 s and 90 s respectively. The measurement results of 479.712 ppm for CO_2 and 331 ppb for N_2O in an indoor environment were obtained, which have shown that the result of the system was in good agreement with the actual situation. This system has great potential in greenhouse gases monitoring.

ACKNOWLEDGMENT

This research was funded by "Pioneer" and "Leading Goose" R&D Program of Zhejiang Province (grant number 2022C03051, 2023C03135), the Key Research and Development Program of Zhejiang Province (grant number 2021C03178), and National Natural Science Foundation of China (11621101). The authors are grateful to Dr. Julian Evans of Zhejiang University for valuable discussions.

REFERENCES

1. Sander, J., J. F. Eichner, E. Faust, and M. Steuer, "Rising variability in thunderstorm-related U.S. losses as a reflection of changes in large-scale thunderstorm forcing," *Weather*, 317–331, 2013.
2. Donat, M. G., A. L. Lowry, L. V. Alexander, P. A. O'Gorman, and N. Maher, "More extreme precipitation in the world's dry and wet regions," *Nature Climate Change*, Vol. 6, 508–513, 2016.
3. Stroeve, J., A. Barrett, M. Serreze, and A. Schweiger, "Using records from submarine, aircraft and satellites to evaluate climate model simulations of Arctic sea ice thickness," *The Cryosphere*, Vol. 8, 1839–1854, 2014.
4. Chen, I-C., J. Donald, Fahey, W. David, Hibbard, and K. Al, "Climate science special report: Fourth national climate assessment, Volume I," *Ecological Research*, 2017.
5. Wuebbles, D., D. R. Easterling, K. Hayhoe, T. Knutson, R. E. Kopp, J. P. Kossin, K. E. Kunkel, A. N. Legrande, C. Mears, and W. V. Sweet, "Our globally changing climate. Chapter 1," *Climate Science Special Report: Fourth National Climate Assessment*, 2017.
6. Melillo, J. M., T. Richmond, G. W. Yohe (eds.) *Climate Change Impacts in the United States: The Third National Climate Assessment*, Vol. 61, No. 12, 46–48, 2014.
7. Kiehl, J. T. and K. E. Trenberth, "Earth's annual global mean energy budget," *Bulletin of the American Meteorological Society*, Vol. 78, No. 2, 1997.

8. Crippa, M., E. Solazzo, D. Guizzardi, F. Monforti-Ferrario, and A. Leip, "Food systems are responsible for a third of global anthropogenic GHG emissions," *Nature Food*, Vol. 2, No. 3, 1–12, 2021.
9. Addington, O., Z.-C. Pongetti, T. Shia, R.-L. Gurney, K. R. Liang, J. Roest, G. He, L. Yung, Y. L. Sander, and P. Stanley, "Estimating nitrous oxide (N_2O) emissions for the Los Angeles Megacity using mountaintop remote sensing observations," *Remote Sensing of Environment: An Interdisciplinary Journal*, Vol. 259, No. 1, 2021.
10. Link, M. S., "Part 7: Adult advanced cardiovascular life support: 2015 American heart association guidelines update for cardiopulmonary resuscitation and emergency cardiovascular care (Vol. 132, S444, 2015)," *Circulation: An Official Journal of the American Heart Association*, 2015.
11. Nunn, J. F. and M. Saklad, "Ventilation and end-tidal carbon dioxide tension a study during routine anaesthesia," *Survey of Anesthesiology*, Vol. 3, No. 3, 261–262, 1959.
12. Nam, H.-J., T. Sasaki, and N. Koshizaki, "Optical CO gas sensor using a cobalt oxide thin film prepared by pulsed laser deposition under various argon pressures," *The Journal of Physical Chemistry B*, Vol. 110, No. 46, 23081–23084, 2006.
13. Elwi, T. A. and W. J. Khudhayer, "A passive wireless gas sensor based on microstrip antenna with copper nanorods," *Progress In Electromagnetics Research B*, Vol. 55, 347–364, 2013.
14. Hu, L., "Research of quartz-enhanced photoacoustic and photothermal spectroscopy-based gas sensing technique," Jilin University, 2021.
15. Xing, Y., G. Wang, T. Zhang, F. Shen, L. Meng, L. Wang, F. Li, Y. Zhu, Y. Zheng, N. He, and S. He, "VOC detections with optical spectroscopy," *Progress In Electromagnetics Research*, Vol. 173, 71–92, 2022.
16. Harren, F., "Laser-based trace gas detection within biology and human health science," *Optical Instrumentation for Energy and Environmental Applications*, 2014.
17. Ren, W., A. Farooq, D.F. Davidson, and R. K. Hanson, "CO concentration and temperature sensor for combustion gases using quantum-cascade laser absorption near 4.7 μm," *Applied Physics*, 2012.
18. Thaler, K. M., C. Berger, C. Leix, J. E. Drewes, R. Niessner, and C. Haisch, "Photoacoustic spectroscopy for the quantification of N_2O in the off gas of wastewater treatment plants," *Analytical Chemistry*, Vol. 89, No. 6, 3795–3801, 2017.
19. Shi, C., D. Wang, Z. Wang, L. Ma, Q. Wang, K. Xu, S. C. Chen, and W. Ren, "A mid-infrared fiber-coupled QEPAS nitric oxide sensor for real-time engine exhaust monitoring," *IEEE Sensors Journal*, Vol. 17, No. 22, 7418–7424, 2017.
20. Zhang, T., G. Zhang, X. Liu, G. Gao, and T. Cai, "A TDLAS sensor for simultaneous measurement of temperature and C_2H_4 concentration using differential absorption scheme at high temperature," *Frontiers in Physics*, Vol. 8, 2020.
21. Cai, T., G. Gao, M. Wang, G. Wang, Y. Liu, and X. Gao, "Simultaneous measurements of temperature and CO_2 concentration employing diode laser absorption near 2.0 μm," *Applied Physics B. Lasers and Optics*, Vol. B118, No. 3, 471–480, 2015.
22. Liu, C. and L. Xu, "Laser absorption spectroscopy for combustion diagnosis in reactive flows: A review," *Applied Spectroscopy Reviews*, 1–44, 2018.
23. Hodgkinson, J. and R. P. Tatam, "Optical gas sensing: A review," *Measurement Science & Technology*, Vol. 24, No. 1, 2013.
24. Hu, L., C. Zheng, Y. Zhang, J. Zheng, and F. K. Tittel, "Compact all-fiber light-induced thermoelastic spectroscopy for gas sensing," *Optics Letters*, Vol. 45, No. 7, 2020.
25. Ma, Y., R. Lewicki, M. Razeghi, and F. K. Tittel, "QEPAS based ppb-level detection of CO and N_2O using a high power CW DFB-QCL," *Optics Express*, Vol. 21, No. 1, 1008, 2013.
26. Yin, X., H. Wu, L. Dong, B. Li, W. Ma, L. Zhang, W. Yin, L. Xiao, S. Jia, and F.K. Tittel, "ppb-level SO_2 photoacoustic sensors with a suppressed absorption-desorption effect by using a 7.41 μm external-cavity quantum cascade laser," *ACS Sensors*, Vol. 5, No. 2, 549–556, 2020.
27. Liu, K., J. Mei, W. Zhang, W. Chen, and X. Gao, "Multi-resonator photoacoustic spectroscopy," *Sensors & Actuators B: Chemical*, Vol. 251, 632–636, Nov. 2017.

28. Gong, Z. F., G. J. Wu, X. Jiang, H. E. Li, T. L. Gao, M. Guo, F. X. Ma, K. Chen, L. Mei, W. Peng, and Q. X. Yu, "All-optical high-sensitivity resonant photoacoustic sensor for remote CH_4 gas detection," *Optics Express*, Vol. 29, No. 9, 13600–13609, 2021.
29. Ma, Y. F., W. Feng, S. D. Qiao, Z. X. Zhao, S. F. Gao, and Y. Y. Wang, "Hollow-core anti-resonant fiber based light-induced thermoelastic spectroscopy for gas sensing," *Optics Express*, Vol. 30, No. 11, 18836–18844, 2022.
30. Kosterev, A. A., A. B. Yu, R. F. Curl, and F. K. Tittel, "Quartz-enhanced photoacoustic spectroscopy," *Optics Letters*, Vol. 27, No. 21, 1902–1904, 2002.
31. Ma, Y. F., "Recent advances in QEPAS and QEPTS based trace gas sensing: A review," *Frontiers in Physics*, Vol. 8, 2020.
32. Ma, Y., Y. Hong, S. Qiao, Z. Lang, and X. Liu, "H-shaped acoustic micro-resonator-based quartz-enhanced photoacoustic spectroscopy," *Optics Letters*, Vol. 3, 47, 2022.
33. Ma, Y., Y. He, X. Yu, C. Chen, R. Sun, and F. K. Tittel, "HCl ppb-level detection based on QEPAS sensor using a low resonance frequency quartz tuning fork," *Sensors & Actuators B: Chemical*, Vol. 233, No. 5, 388–393, 2016.
34. Wu, H., A. Sampaolo, L. Dong, P. Patimisco, X. Liu, H. Zheng, X. Yin, W. Ma, L. Zhang, W. Yin, V. Spagnolo, S. Jia, and F.K. Tittel, "Quartz enhanced photoacoustic H2S gas sensor based on a fiber-amplifier source and a custom tuning fork with large prong spacing," *Applied Physics Letters*, Vol. 107, No. 11, 2015.
35. Qiao, S. D., A. Sampaolo, P. Patimisco, V. Spagnolo, and Y. F. Ma, "Ultra-highly sensitive HCl-LITES sensor based on a low-frequency quartz tuning fork and a fiber-coupled multi-pass cell," *Photoacoustics*, Vol. 27, 2022.
36. He, Y., Y. Ma, Y. Tong, X. Yu, and F. K. Tittel, "Ultra-high sensitive light-induced thermoelastic spectroscopy sensor with a high Q-factor quartz tuning fork and a multipass cell," *Optics Letters*, Vol. 44, No. 8, 1904–1907, 2019.
37. Ma, Y., Y. Hu, S. Qiao, Y. He, and F. K. Tittel, "Trace gas sensing based on multi-quartz-enhanced photothermal spectroscopy," *Photoacoustics*, Vol. 20, 100206, 2020.
38. Zhang, Q., J. Chang, Z. Cong, and Z. Wang, "Long-path quartz tuning fork enhanced photothermal spectroscopy gas sensor using a high power Q-switched fiber laser," *Measurement*, Vol. 156, 107601, 2020.
39. Zhou, S., L. Xu, K. Chen, L. Zhang, B. Yu, T. Jiang, and J. Li, "Absorption spectroscopy gas sensor using a low-cost quartz crystal tuning fork with an ultrathin iron doped cobaltous oxide coating," *Sensors and Actuators B: Chemical*, Vol. 326, 2020.
40. Hu, Y. Q., S. D. Qiao, Y. He, Z. T. Lang, and Y. F. Ma, "Quartz-enhanced photoacoustic-photothermal spectroscopy for trace gas sensing," *Optics Express*, Vol. 29, No. 4, 5121–5127, 2021.
41. Rothman, L. S., I. E. Gordon, Y. Babikov, and A. Barbe, "The HITRAN2016 molecular spectroscopic database," *Journal of Quantitative Spectroscopy & Radiative Transfer*, Vol. 130, No. 11, 4–50, 2017.